End-point energies of electrons ejected during Auger neutralization of slow, multicharged ions near metal surfaces

R. H. Hughes, Garvin Wattuhewa, R. D. Miller, X. M. Ye, and D. O. Pederson
Physics Department, University of Arkansas, Fayetteville, Arkansas 72701
(Received 6 April 1987)

A study has been done of the end-point energies of electrons ejected during Auger neutralization of slow, multicharged ions near metal surfaces. The study includes a wide variety of ions. Experimental results are presented for Al^{z+} and C^{n+} ions incident on a gold surface, where $z=2-5$ and $n=2-5$. Ions from a laser-ion source are processed to produce ion pulses with incident energies ranging from 40 to 280 eV/charge. Data published by Hagstrum for 200-eV He^{2+}, Ne^{n+}, Ar^{n+}, Kr^{n+}, and Xe^{n+}, on tungsten, where $n=2$ and 3, are analyzed along with the work of Varga, Hofer, and Winter for low-energy Ne^{2+}, Ar^{2+}, Ar^{3+}, Kr^{2+}, and Xe^{2+} on tungsten. It is concluded that the high-energy end of the Auger emission is dominated by single-electron capture by the ion and an internal conversion process involving direct coupling of optically allowed transitions in the lower-lying excited states of the singly neutralized ion to the top of the conduction band of the metal target. It is shown that a considerable fraction of the neonlike Al^{3+} ions from the laser-ion source are in a metastable state and are neutralized through autoionization.

INTRODUCTION

The first definitive study of Auger neutralization of slow ions near metal surfaces was published by Hagstrum[1,2] in 1954. In the first of these classic papers, he presented experimentally determined electron yields and energy distributions of electrons ejected during the neutralization of slow rare-gas ions near an atomically clean tungsten surface.[1] In the second paper[2] he gave a theoretical analysis of his experimental results for singly charged ions. However, Hagstrum's published data also included the results for electrons ejected in the neutralization of the multicharged ions He^{2+}, Ne^{m+}, Ar^{m+}, Kr^{n+}, and Xe^{p+} where $m=2-3$, $n=2-4$, and $p=2-5$. From an analysis of the electron yields Hagstrum concluded that neutralization of multiply charged ions near a surface is likely to occur in a series of stages where each stage excites an electron inside the metal. No analysis of the end-point energies was performed. More recently, Varga *et al.*[3] have obtained higher-resolution spectra of Auger electron energies produced by ≤ 30-eV Ne^{2+}, Ar^{2+}, Ar^{3+}, Kr^{2+}, and Xe^{2+} impact on tungsten.

Arifov *et al.*[4] have treated Auger neutralization of multiply charged ions near a metal surface, pointing out the ion can undergo a series of resonant and Auger neutralizations to high-lying excited states as the ion approaches the metal. Figure 1 schematically shows Auger neutralization where an electron is captured from the conduction band into an excited state of the singly neutralized ion. Any loss in excitation energy during the neutralization process goes into exciting another electron in the conduction band. If the excitation energy transfer to the conduction-band electron is sufficient and its momentum is properly directed toward the surface, then it may escape the potential well at the surface and be detected as an Auger-emitted electron. The ejected electron may have lost energy in collisions with the conduction electrons before finding itself free of the surface.[5] Thus the end-point energy electron in the broad energy spectrum of the emitted electrons provides a unique probe of the neutralization processes. These end-point energy electrons are the ones that have been given initially the maximum energy transfer in the neutralization process, have suffered little collisional loss with other conduction electrons, and have their origin in the top of the conduction band where the potential well depth is the work function ϕ. These electrons thus have reason-

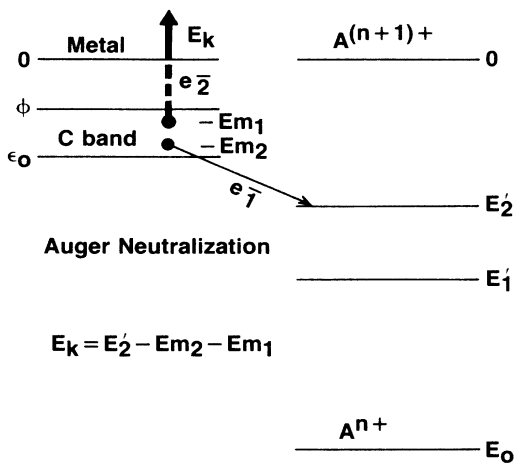

FIG. 1. Schematic diagram of the Auger neutralization process. The slow ion carrying a charge of $(n+1)+$ is incident on the metal surface. When the ion comes sufficiently close to the surface, electron capture from the conduction band takes place with the simultaneous ejection of the second electron with a kinetic energy E_k as measured at a distance from the surface. E_0 is the ground state of the singly neutralized ion.

ably well-defined energies.

Arifov *et al.* point out that the maximum energy transferred to the ejected electrons is a measure of the largest energy gap spanned in the downward atomic transition. They further point out that the Auger transition rates to low-lying levels of the neutralizing ion are small, since the overlap of the wave function of the metal electron with the atomic electron wave function grows smaller as the energy difference between the metal electron and the atomic electron grows larger. Thus direct Auger transitions to the ground state and first excited states of atoms that carry large neutralization energies are not likely. In their paper they suggest that autoionization is an alternative way to arrive at the ground state. Figure 2 illustrates their concept of possible autoionization processes. Double capture takes place, producing a doubly excited state of the twice-neutralized ion. Since the doubly excited state lies above the ground state of the singly neutralized ion, coupling occurs between the continuum states of the doubly neutralized ion, resulting in autoionization and the ejection of one of the electrons, leaving the ion in a singly neutralized state. Arifov *et al.* calculated the end-point energies expected from double capture followed by autoionization using Hagstrum's 1954 data for comparison. They assumed the energy of the ejected electron would be given by $E_k \simeq E_0 - 2E_1''$, using the single-electron nomenclature of Fig. 2. [This is a valid expression in the case $E_1'' \simeq E_2''$. As seen in Fig. 2, a more exact expression is simply $E_k = E_0 - (E_1'' + E_2'')$, where E_1'' and E_2'' are the binding energies of each of the two electrons.] In Ref. 4, the binding energy E_1'' is calculated using a method developed by Slater[6] where a Rydberg hydrogenlike expression is used for the binding of an electron in a given electron shell by estimating the nuclear charge shielding by electrons in the inner shells and by electrons in the same shell, the shells being described by the principal and orbital quantum numbers. The shielding parameters were determined empirically by Slater. However, the Slater calculation is not meant to be a precision method for determining specific binding energies but only a general technique for estimating these energies. For example, equivalent s and p electrons are treated as having the same shielding parameters.

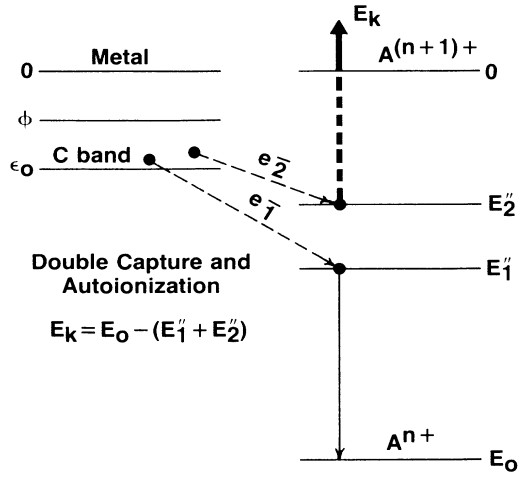

FIG. 2. Schematic diagram of the double-capture process with autoionization taking place in a doubly neutralized ion, resulting in the ejection of an electron with kinetic energy E_k.

APPARATUS

Figure 3 shows the general scheme of the apparatus. The scheme is similar to that used by Phaneuf[7] in the study of charge exchange with gas targets. A 50-MW Nd-YAG laser (where YAG represents yttrium aluminum garnet) is focused on a cylindrical laser target. (The principal aspects of the laser-ion source have been described previously.[8]) The laser pulse produces a plasma plume that advances to the entrance of a 180° electrostatic analyzer where a 100-mesh stainless-steel screen strips the electrons from the plasma. The ions that have been selected by the analyzer emerge as ion packets with a given kinetic energy per charge. The ions pass through an ion gate where an optional timed pulse can be applied to select a particular ion charge. The ions then impinge on the surface of a gold target. (The ion flight path is about 135 cm to the target.) The target chamber contains a channeltron electron multiplier array (CEMA) detector which can operate either in an ion detector mode or an electron detector mode. The projectile particles that are specularly scattered through a 45° angle of deviation may continue on through an analyzer arm where collisional energy loss and charge change are determined.[9] The present paper is restricted to the analysis of Auger electrons ejected in the neutralization of the multicharged projectiles near the ion target surface and only makes use of the CEMA detector in the target chamber (see Fig. 3).

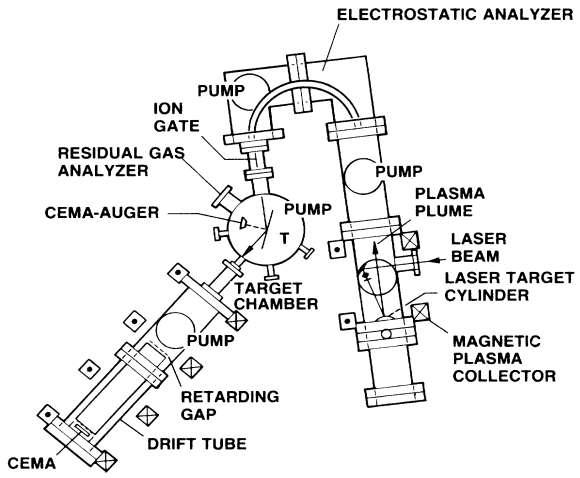

FIG. 3. Schematic diagram of the laser-ion source apparatus. The parts pertinent to this paper include the ion source through to the target chamber. The arm extending from the target chamber to the extremity containing the second CEMA detector is used for charge neutralization experiments (Ref. 9).

The gold target surface is uncharacterized. Base pressures are a few times 10^{-9} Torr in the collision chamber. Pumping is supplied by two 170-l/s turbomolecular pumps and a 140-l/s diode ion pump. Base pressures are reached by employing a 1000-l/s Varian Ti-ball pump in the collision chamber. The Ti-ball pump is turned off during data taking in order to minimize the electron background. The remaining pumping is sufficient to maintain the base pressure. However, the pumping is not sufficient to keep up with the photodissociation products produced in the ion source operating at a 6-Hz repetition rate. The pressure then rises above 5×10^{-8} Torr.

In order to demonstrate that we are truly observing Auger electrons from potential ejection rather than a kinetic ejection mechanism,[10] it was necessary to obtain data from the slowest possible ions. A special collision box was constructed which permitted the application of a retarding potential to further slow the ions before impact on the target surface. The box is shown in Fig. 4. Ion collisions with the surface take place in a field-free environment with the help of stainless-steel screens. An ion-retarding gap is defined at S_1S_2 and an electron-retarding gap is defined at S_3S_4. The well-shielded Galileo CEMA operates with the collector at high positive potential.

The Auger electron signal is fed to a LeCroy WD8256 waveform digitizer through a preamplifier and a timing amplifier. Data acquisition is initiated by a Commodore PET computer which fires the laser through an optical link. A stop trigger is supplied to the digitizer through another optical link by picking off a small fraction of the laser light. Data accumulated in the digitizer memory are then transferred to the computer memory for readout and data processing. The rate of data acquisition is computer limited to about 6 Hz and should be laser limited to about 20 Hz.

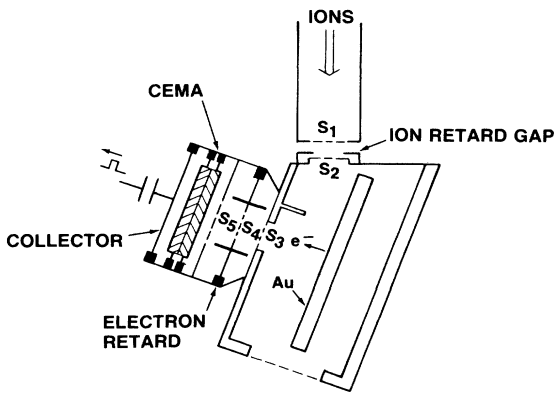

FIG. 4. Schematic diagram of the insulated Faraday cage containing the gold target and the Auger electron-retarding fields. The CEMA view is normal to the target surface. The impacting ions are incident at an angle of about 20° to the target surface.

RESULTS

Auger emission induced by sufficiently slow ion impact occurs on the *incoming* pass[11] before the ion strongly interacts with the surface. It is therefore reasonable to assume that the ion time-of-flight (TOF) linewidths as perceived by the Auger detector should reflect the actual energy widths within the ion packets striking the gold surface. The relative energy width of each ion packet is given as $\Delta E/E=2\Delta t/t$, where E is the ion kinetic energy and t is the ion time of flight. The energy resolution of the analyzer is measured by the angular cone of ions streaming from the analyzer that is actually accepted by an ion detector.[12] The relative linewidth scales directly with the acceptance cone. The energy resolution of the analyzer is calculated to be $\Delta E/E=4.5\%$, using the full exit aperture. The relative linewidth using the actual acceptance cone of the Auger detector is estimated to be about $\Delta E/E=2.0\%$. Figure 5 shows the ion spectra emanating from the analyzer, using the Auger detector, and the effect of applying the magnetic field on the laser side of the analyzer (Fig. 3). The signals are negatively directed peaks with positive overshoots produced by amplifier overdrive. The overshoots were useful in recognizing the presence of small signals. Figure 5(a) shows the ion spectra produced by 280-eV/charge carbon without the magnetic field, while Fig. 5(b) shows the spectra with the magnetic field. Notable features are the broader linewidths, the appearance of C^{5+}, and the absence of C^{1+} of Fig. 5(b) relative to Fig. 5(a). The linewidths ($\Delta E/E$) in Fig. 5(a) run from about 2.8% for C^{2+} to about 3.8% for C^{4+}, while in Fig. 5(b) they run

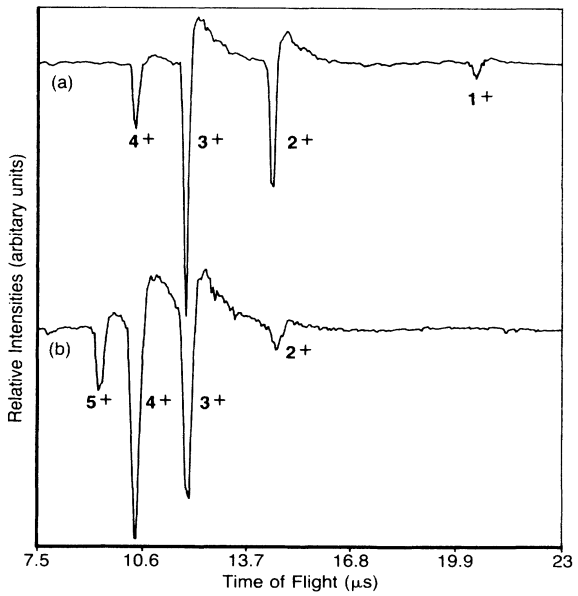

FIG. 5. Carbon ion spectra emanating from the electrostatic analyzer using the Auger electron detector shown in Fig. 4. The energy selected is 280 eV/charge and the Faraday cage is grounded so that the ions are not retarded. In Fig. 5(a) the magnetic ion collector shown in Fig. 3 is not in use. In Fig. 5(b) the magnetic collector is in use.

from about 4.2% for C^{2+} to about 6.4% for C^{5+}. Our interpretation of the increase in linewidth with increase in charge state is that it is evidence of longitudinal space-charge repulsion effects in the ion packets. [The effect is present in our apparatus when the ion packets are observed straight from the analyzer exit with no interaction with surfaces. It is also noticed in the linewidths in the Oak Ridge National Laboratory (ORNL) laser-ion source experiments.[7]] The increase in linewidth with the application of the laser-side magnetic field is due to plasma loading effects in the analyzer which not only broaden the ion lines but also slow the ions down. This broadening is not very apparent in Fig. 5 but is quite noticeable in the longer flight times using aluminum ions (Fig. 6). The dense plasma partially shields the ions from the analyzer electric field reducing the effective field. (The analyzer plates are kept at a constant voltage despite the large current drawn when the plasma enters the analyzer by capacitively loading the power supply.) The axial magnetic field has the effect of enhancing the highest charge content in the plasma at the analyzer entrance and it should also enhance the C^{1+} content.[8] The apparent absence of C^{1+} in Fig. 5(b) is probably not because of a paucity of C^{1+} ions but because the application of the magnetic field produces a weak stray field inside the collision chamber which magnetically insulates the Auger detector from the low-energy (~ 1 eV) electrons ejected by C^{1+}. Experimentally we find that it has little effect on electrons ejected at energies above 10 eV.

Figures 6(a) and 6(b) display TOF spectra for 280-eV/charge aluminum ions. The TOF for these heavier ions is scaled by the square root of the mass ratio to be 1.5 times slower than the carbon ions. Figures 6(a) and 6(b) again show the effects of the magnetic field described for Fig. 5. The ion lines are again broadened. Here it is obvious that the application of the magnetic field has actually slowed the ions, supporting the concept of plasma loading in the analyzer which reduces the effective electric field affecting the ions.

In Figs. 6(c) and 6(d) an ion-retarding potential of 200 V has been applied to the box, allowing 80-eV/charge ions into the box. In Figs. 6(c) and 6(d) it is seen that each of the ion lines splits into two parts. There is the expected Auger emission from the gold target occurring at a later time since the ions have been slowed from 280 eV/charge to 80 eV/charge. (Data have been taken as low as 40 eV/charge.) Each ion line also has a precursor labeled "sec" which is caused by ion impact outside the box producing secondary electrons which are accelerated through the 200-V potential into the box and subsequently detected. Thus the target surface is sprayed with 200-eV electrons before each ion packet arrives at the surface.

Figure 7 shows the application of the electron-

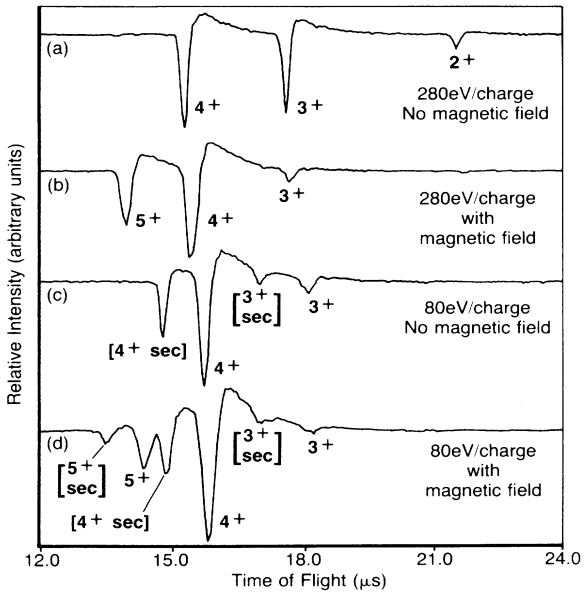

FIG. 6. Aluminum ion spectrum as seen by the Auger detector shown in Fig. 4. (a) The cage is grounded with the magnetic collector not in use. (b) The cage is grounded with the magnetic collector in use. (c) The cage has + 200 V applied to it so that the energy of the ions entering the cage is 80 eV/charge, no magnetic field is applied to the laser plasma. The peaks labeled "sec" are artifacts induced by the cage potential (see text). (d) The cage is held at the same potential as in (c) but with the magnetic field applied.

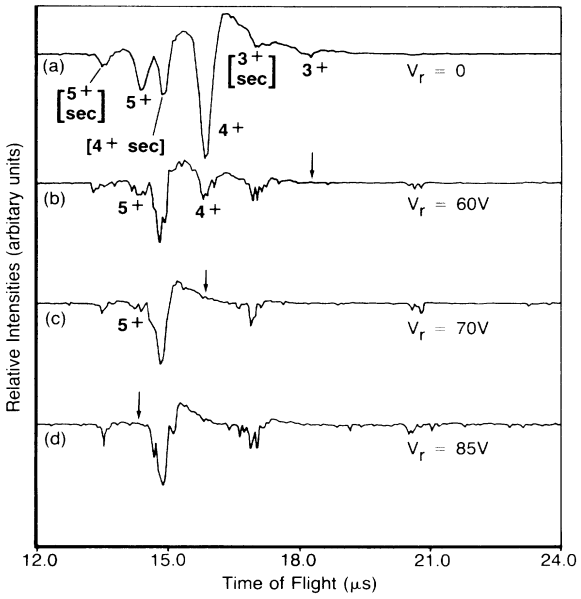

FIG. 7. Electrons detected in the Faraday cage using aluminum ions. The magnetic collector is in use. The cage has + 200 V applied to it so that 80-eV/charge ions enter the box. (a) No potential is applied to the electron-retarding grid. (b) A potential of −60 V relative to the box is applied to the electron-retarding grid. The arrow marks the disappearance of the Auger electrons ejected by Al^{3+} metastable ions near the gold surface. (c) A potential of −70 V relative to the box is applied to the retarding grid. The arrow marks the disappearance of the Auger electrons ejected during the neutralization of Al^{4+} ions near the gold surface. (d) A potential of −85 V is applied to the grid; the arrow marks the disappearance of Auger electrons induced by the Al^{5+} ions.

retarding field on the Auger signals for 280-eV/charge aluminum ions. Here the goal is to determine the end-point energy of the electrons being ejected from the ion-metal systems. The technique used here is to apply sufficient potential to totally stop the electron emission. The point where the signal is totally gone defines the end-point energy. The present generation of data from the laser-ion source is not sufficiently reproducible to obtain relative electron yields as a function of energy and to extrapolate to precise end-point energies. The present technique will generally tend to produce an underestimate in the end-point energies, in particular when the initial electron yields are low. However, in our judgment the end-point energies quoted here will be at most underestimated by 3 eV. This judgment is based on well over 100 data runs, generally involving multiple ion Auger signatures per run. Each signature represented data accumulated from 50 to 200 laser shots. These data were obtained primarily over the ion kinetic energy range from 40 eV/charge to 280 eV/charge. No systematic difference could be found in the electron end-point energies in this ion kinetic energy range. If any kinetic effect produces secondary electrons in this range, it produces electrons with kinetic energies less than 10 eV. The maximum energy of electrons ejected during Auger neutralization (Fig. 1) is $E_{k\,\max}=E_0-2\phi$. For Al^{1+} incident on gold, $E_0=6.0$ eV (Ref. 13) and $\phi=5.1$ eV.[14] Thus Al^{1+} cannot eject electrons by virtue of the potential energy that it carries. An electron signature from Al^{1+} never occurred in our work until the ion energy reached 560 eV and it vanished when the magnetic field was turned on, consistent with the concept of magnetic insulation of low-energy electrons.

The importance of the end-point energies of the Auger energy spectrum lies in the fact that they give a reasonably well-defined energy which involves the ejection of the least bound of the metal electrons; namely, electrons at the top of the conduction band. The most energetic of the Auger electrons by definition involves an electron that does not experience an energy-loss collision with other electrons in the conduction band. Finally, the most energetic Auger electron is one in which the largest possible energy transfer in the neutralization process has been made.

In Table I we offer the end-point energies for Auger-ejected electrons induced by eight different multicharged ions on gold along with the analysis of end-point energies of nine different multicharged ions on tungsten as measured by Hagstrum and Varga *et al.* We offer one mechanism as the explanation for neutralization of 16 of the 17 cases. The single exception occurs in Al^{3+}, which is complicated by the fact that a large fraction of the Al^{3+} ion packets produced in the ion source is in a metastable state. The total neutralization energy for Al^{3+} in the ground state going to Al^0 in the ground state is only 53.5 eV. Table I shows the end-point energy of electrons ejected by our Al^{3+} packets is 60 eV. Even in the unlikely event that all the neutralization energy was somehow given to a single electron, there would be a 7-eV discrepancy. The most probable explanation is that Al^{3+} is a neonlike ion in which there is a metastable state lying 76.5 eV *above* the Al^{3+} ground state. If an appreciable number of the incident Al^{3+} ions are in this state, we have a total neutralization energy of 129.8 eV instead of 53.3 eV. The Al^{3+} ion is listed as $Al^{3+}(m)$ in Table I.

The second column in Table I lists the maximum Auger energy expected from Auger neutralization where an electron from the top of the conduction band drops to the ground state of the singly neutralized ion with the subsequent ejection of another electron from the top of the conduction band. As can be seen, this calculated energy greatly overestimates the actual experimentally determined end-point energy for multicharged ions. This fact is not surprising, using the argument of Arifov *et al.* that the overlap in the deep-lying ground state and conduction-band wave functions is too small to make this an effective mechanism.

Another choice is double capture from the conduction band into a doubly excited state of the twice-neutralized ion with subsequent Auger ejection from the atom leaving the ion in the ground state of the singly neutralized ion (Fig. 2). Arifov *et al.* argue that the end-point energies are obviously due to transitions involving energy levels with large gaps which typically occur in the lower-energy states. For example, consider the case of Ne^{3+} incident on a metal. The ground state of Ne^{3+} has the electron configuration $1s^2 2s^2 2p^3$. If double capture takes place, it is most probable that it is autoionization in the $n=3$ doubly excited states of Ne^{1+} that is responsible for the end-point energies. The binding energies are calculated by Slater's method. Thus a likely configuration of $1s^2 2s^2 2p^3 3s^2$ might result with one $3s$ electron being ejected and the other falling into another $2p$ orbital, resulting in the $1s^2 2s^2 2p^4$ ground-state configuration of Ne^{2+}. The results of the calculations of Arifov *et al.* are listed in the last column of Table I. Notable disagreements occur in the case of Ne^{3+} and Ne^{2+}.

Burhop[15] has shown that Auger ejection can be treated in a nonrelativistic fashion as an internal conversion process in which the radiation field set up when one electron drops to a lower energy then acts as a perturbation to excite the second electron. Suggesting that it is the radiation field that couples the two electrons in the ion-metal system allows us to view the Auger ejection in Fig. 1 as a photoelectric conversion in the conduction band.[16] Such conversion processes are well known in the interpretation of x-ray spectra of solids where Coster-Kronig transitions allow core electron excitation to be coupled to the conduction band in metals.[15] Figure 8(a) shows schematically the direct Auger deexcitation using optically allowed transitions in the singly neutralized ion. Figure 8(b) shows schematically the corresponding exchange transition. We may again use the argument of Arifov *et al.* that the overlap in wave functions involving the low-lying atomic states is too small to make such exchange reactions prevalent. Thus an internal conversion process involving optically allowed transitions seems a real possibility. We offer the results from such a process in the column labeled "Auger deexcitation" and the transitions responsible for the calculated end-point

-0002-

TABLE I. End-point energies of electrons ejected during Auger neutralization of slow multicharged ions near metal surfaces.

Pairs	Auger neutralization[a] $E_1-2\phi$ (eV)	Experiment[b] (eV)		Energy (eV)	Auger deexcitation Transition	Autonization (eV)	This work	Arifov (eV)
$C^{2+}+Au$	14.2	10		9.3	$C^+\ 2s^2 3s\ (^2S)\rightarrow 2s^2 2p\ (^2P^\circ)$	13	$C^0(3s^2\rightarrow 2p\,\infty)$	
$C^{3+}+Au$	37.7	18		17.9	$C^{2+}\ 2s3s\ (^3S)\rightarrow 2s2p\ (^3P^\circ)$	24	$C^+(3p^2\rightarrow 2s\,\infty)$	
$C^{4+}+Au$	54.3	36		34.6	$C^{3+}\ 1s^2 3p\ (^2P^\circ)\rightarrow 1s^2 2s\ (^2S)$	24	$C^{2+}(3p^2\rightarrow 2s\,\infty)$	
$C^{5+}+Au$	381.8	>200[d]		299.2	$C^{4+}\ 1s2p\ (^1P^\circ)\rightarrow 1s^2\ (^1S)$	235	$C^{3+}(2p^2\rightarrow 1s\,\infty)$	
$Al^{2+}+Au$	8.6	<5		4.8	$Al^+\ 2p^6 3s3p\ (^1P^\circ)\rightarrow 2p^6 3s^2\ (^1S)$	12	$Al^0(4p^2\rightarrow 3s\,\infty)$	
$Al^{3+}(m)+Au$		60				62.7[e]		
$Al^{4+}+Au$	109.8	70		72.4	$Al^{3+}\ 2p^5\ (^2P^\circ)3s\rightarrow 2p^6\ (^1S)$	93	$Al^{2+}(4s^2\rightarrow 2p\,\infty)$	
$Al^{5+}+Au$	143.6	85		89.6	$Al^{4+}\ 2p^4 3s\ (^2P)\rightarrow 2p^5\ (^2P^\circ)$	61	$Al^{3+}(3s^2\rightarrow 2p\,\infty)$	
		Hagstrum	Varga					
$He^{2+}+W$	45.4	35		36.3	$He^+\ 2p\ (^2P^\circ)\rightarrow 1s\ (^2S)$	36	$He^0(2p^2\rightarrow 1s\,\infty)$	
$Ne^{2+}+W$	32.1	28	30	29.8	$Ne^+\ 2p^4 3s''\ (^2S)\rightarrow 2p^5\ (^2P^\circ)$			21
$Ar^{2+}+W$	18.6	17	19	16.2	$Ar^+\ 3p^4 4s''\ (^2S)\rightarrow 3p^5\ (^2P^\circ)$			15
$Kr^{2+}+W$	15.6	13	16	13.6	$Kr^+\ 4p^4 5s''\ (^2S)\rightarrow 4p^5\ (^2P^\circ)$			13
$Xe^{2+}+W$	12.2	11	14.5	10.9	$Xe^+\ 5p^4 6s''\ (^2S)\rightarrow 5p^5\ (^2P^\circ)$			10
$Ne^{3+}+W$	55	40		41.9	$Ne^{2+}\ 2p^5 3s''\ (^3P^\circ)\rightarrow 2p^4\ (^3P)$	29	$Ne^+(3s^2\rightarrow 2p\,\infty)$	29
$Ar^{3+}+W$	31.9	25	26	21.2	$Ar^{2+}\ 3p^5 4s''\ (^3P^\circ)\rightarrow 3p^4\ (^3P)$			18
$Kr^{3+}+W$	27.9	19		17.6	$Kr^{2+}\ 4p^5 5s''\ (^3P^\circ)\rightarrow 4p^4\ (^3P)$			16.4
$Xe^{3+}+W$	23.1	15		14.2	$Xe^{2+}\ 5p^5 6s''\ (^3P^\circ)\rightarrow 5p^4\ (^3P)$			14.3

[a]Transition to the atomic ground state from the top of conduction band.

[b]The gold target data are uncorrected for contact potentials (see text).

[c]Calculated for double capture (see text) except for $Al^{3+}(m)$.

[d]Circumstances did not allow completion of the measurement. The end-point energy is well above 200 eV.

[e]The $Al^{3+}(3s\ ^3P)$ metastable ion captures a conduction electron into a doubly excited state of Al^{2+}. Estimated value of end-point energy is for $Al^{2+}(2p^5 3s3d)\rightarrow Al^{3+}(2p^6)+e^-$ (see text).

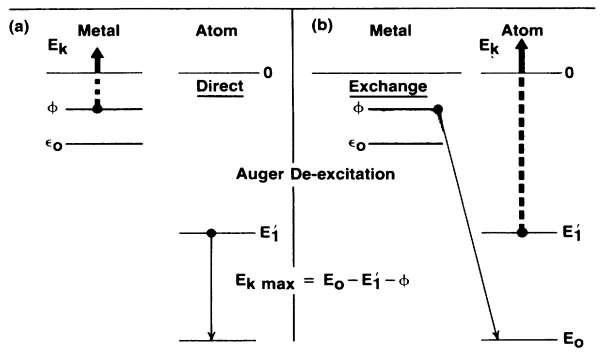

FIG. 8. Schematic representation of the Auger ejection by atom deexcitation. Shown in (a) is ejection from the top of the conduction band. (b) represents the corresponding exchange reaction. Both reactions involving electrons from the top of the conduction band produce the maximum energy of ejection.

energies. These transitions have been selected according to the following model. Auger neutralization takes place in the upper excited states of the singly neutralized ion. The electron cascades to the lower excited states. The excitation energy is most likely lost in exciting other conduction electrons. (We have actively searched for optical radiation without success. Hagstrum[2] has pointed out that optical transitions have transition rates that are too slow to compete with the Auger processes in ordinary atoms. However, these transition rates increase in multicharged systems.) The atomic electron responsible for the end-point Auger energy is that which ends up in the lowest optically active orbital that has a principal quantum number one greater than that of the valence electron associated with the ground state and that which makes a transition to the lowest optically connected state (usually the ground state), if this transition is coupled to an electron at the top of the conduction band. The end-point energy is then $E_{k\,\max}=E_t-\phi$, where E_t is the transition energy and $\phi=5.1$ and 4.5 eV is the work function for gold and tungsten, respectively.

The case of C^{3+} on Au is interesting. The ground state of C^{2+} is the $1s^2 2s^2$ (^1S) state. If transitions to the ground state dominated the production of high-energy Auger electrons, then it would be the $1s^2 2s 3p$ ($^1P^\circ$)$\rightarrow 1s^2 2s^2$ (^1S) transition that would produce a 27-eV end-point energy electron. However, the C^{2+} optical spectrum in the vacuum ultraviolet region[17] shows a rich, well-developed set of triplet transitions with optical power that dominates the singlet system. Thus the Auger emission must show that dominance and it is the triplet transition $1s^2 2s 3s$ (^3S)$\rightarrow 1s^2 2s 2p$ ($^3P^\circ$) that controls the apparent 18-eV end-point energy. The $1s^2 2s 2p$ ($^3P^\circ$) state is the lowest-lying triplet state and is 6.5 eV above the ground state. The C^{3+} entry in Table I is unique in that it is the only one that does not involve transitions to the ground state.

The deexcitation of $Al^{3+}(m)$ also follows the argument that only optically allowed transitions play a dominant role in the end-point ejection process for multicharged ions. The Al^{3+} $1s^2 2s^2 2p^5 3s$ (^3P) neonlike state is metastable because an optical transition to the singlet ^1S ground state is spin forbidden. If an exchange reaction took place, an end-point energy of $76.5-5.1=71.4$ eV might be expected. The experimental value is about 60 eV, well below 71.4 eV. The explanation is that the $Al^{3+}(m)$ ion must lose its energy by capturing another electron, producing a doubly excited state of Al^{2+}. The electron cascades to an $n=3$ orbital where a strong interaction exists with the excited $3s$ orbital already associated with the metastable state. Since Slater's method for calculating binding energies may not be sufficiently accurate for our purposes, we choose to estimate the autoionization energy in the following fashion. If the captured electron falls into a $3d$ orbital, then its shielding of the ion charge which affects the $3s$ orbital is minimal. Thus the binding energy of the Al^{2+} $1s^2 2s^2 2p^5 3s 3d$ configuration can be approximated by using the tabulated experimental binding energies[13] of $Al^{2+}(3d)$ and $Al^{3+}(3s)$. Good agreement between autoionization and experiment is brought about by using this approximation as the binding energy of the autoionizing $3s 3l$ doubly excited state of Al^{2+}. Using Slater's method, the autoionizing $3s^2$ (or $3s 3p$) and $3s 3d$ states of Al^{2+} give end-point energies of 53.2 and 67.9 eV, respectively.

EFFECT OF CONTACT POTENTIAL AND TARGET WORK FUNCTION ON THE END-POINT ENERGIES

The effect of contact potential and possible differences between the actual work function of our formally untreated gold target and the clean surface work function have been neglected in the foregoing analysis for the sake of clarity. Both effects produce changes that are typically a fraction of an electron volt and would be difficult to detect with the present apparatus. Our target surface has been subjected to an extended bakeout at $\sim 180\,^\circ$C, to a bath in vacuum ultraviolet light from the intense laser-produced plasma radiation that reflects through the 180° analyzer (100-eV photoelectrons are produced from the gold surface at each laser fire), to 200-eV secondary electron impact, and finally to ion impact. However, for the case of Auger deexcitation, the work function for the target does not formally enter into the actual measurement. The experimental value of the end-point energy is formally given as

$$E_{k\,\max}=E_t-\phi+(\phi-\phi_s)=E_t-\phi_s\ ,$$

where ϕ is the target work function and ϕ_s is the work function of the stainless-steel retarder grid. The quantity $\phi-\phi_s$ is the contact potential.[18] Thus it is the work function of the stainless steel that should be used to reduce the transition energy and not the gold. The work function for stainless steel, which has undergone heating similar to our grid, has been measured with values that cluster about 5.1 eV.[19] This is the numerical value used in the analysis. Thus the analysis presented here should be valid within experimental error.

SUMMARY AND CONCLUDING REMARKS

The end-point energies of electrons ejected during the neutralization of slow, multicharged carbon and alumi-

num ions near a gold surface have been measured. Analysis of the end-point energies suggests that neutralization is stepwise where a single electron is captured from the metal conduction band which then cascades through the energy levels of the once neutralized ion, losing its energy through excitation of other conduction-band electrons. The end-point Auger electrons are produced in the last stages of this energy-loss ladder when the singly neutralized ion is near its ground state. There is no evidence of exchange reactions taking place in these last stages. There is no evidence of multiple capture processes in the end-point electrons. The end-point energy electrons, however, may not be the electrons that would best reflect such processes, since the neutralization energy per captured electron is reduced by each capture event. Finally, it is not apparent that the end-point energy electrons from neutralization of charge number ≤ 5 ions as yet reflect an appreciable compression of the atomic energy levels by the image potentials.[2] The attractive image potential energy in eV produced by an ion of charge number Z in front of a perfect conductor is $3.6Z^2/S$ where S is the ion-surface distance measured in angstroms. Thus the image forces on the neutralization $Z+ \rightarrow (Z-1)+$ should effectively *reduce* the kinetic energy of the Auger-ejected electron as the electron makes the transition from the initial *metal*$-Z+$ *ion* potential curve to the final *metal*$-(Z-1)+$ *ion* potential curve by an amount $(2Z-1)3.6/S$ eV. However, the end-point energy electrons by definition represent capture at "large" distances from the surface and thus are not particularly sensitive to these energy shifts. These capture distances may also increase with the incident charge since the range of the Coulomb force is increasing.

ACKNOWLEDGMENT

The research described here has been supported by the National Science Foundation through Grant No. DMR-8576109, jointly funded by the Atomic, Molecular, and Plasma Physics Program and the Solid State Physics Program.

[1]H. D. Hagstrum, Phys. Rev. **96**, 325 (1954).
[2]H. D. Hagstrum, Phys. Rev. **96**, 336 (1954).
[3]P. Varga, W. Hofer, and H. Winter, Surf. Sci. **117**, 142 (1982).
[4]U. A. Arifov, L. M. Kishinevskii, E. S. Mukhamadiev, and E. S. Parilis, Zh. Tekh. Fiz. **43**, 181 (1973) [Sov. Phys.—Tech. Phys. **18**, 118 (1973)].
[5]P. A. Wolff, Phys. Rev. **95**, 56 (1954).
[6]J. C. Slater, Phys. Rev. **36**, 57 (1930).
[7]R. A. Phaneuf, IEEE Trans. Nucl. Sci. **NS-28**, 1182 (1981).
[8]L. G. Gray, R. H. Hughes, and R. J. Anderson, J. Appl. Phys. **53**, 6628 (1982).
[9]R. H. Hughes, X. M. Ye, and D. O. Pederson, Appl. Phys. Lett. **47**, 1282 (1986).
[10]For example, J. Ferron, E. V. Alonso, R. A. Baragiola, and A. Oliva-Florio, J. Phys. D **14**, 1707 (1981).
[11]H. D. Hagstrum, in *Inelastic Ion-Surface Collisions*, edited by N. H. Tolk, J. C. Tully, W. Heiland, and C. W. White (Academic, New York, 1977), p. 1.
[12]F. R. Paolini and G. C. Theodoridis, Rev. Sci. Instrum. **38**, 579 (1967).
[13]*Atomic Energy Levels*, Natl. Bur. Stand. (U.S.) Cir. No. 467, compiled by C. E. Moore (U.S. GPO, Washington, D.C., 1949), Vol. I.
[14]*Handbook of Chemistry and Physics*, edited by R. C. Weast (CRC, Boca Raton, 1985), p. E-86.
[15]E. H. S. Burhop, *The Auger Effect and Other Radiationless Transitions* (Cambridge University Press, Cambridge, England, 1952).
[16]F. M. Propst, Phys. Rev. **129**, 7 (1963).
[17]*Atomic Emission Lines Below 2000 Angstroms*, NRL Report No. 6648, compiled by R. L. Kelly (U.S. GPO, Washington, D.C., 1968).
[18]J. A. Bearden and A. F. Burr, Rev. Mod. Phys. **39**, 125 (1967).
[19]A. J. Szadkowsky, A. Kalnitsky, K. B. Ma, and S. Zukotynski, J. Appl. Phys. **53**, 557 (1982).